Supporting information

for

Comprehensive Evaluation of Models for Ammonia Binding to the Oxygen Evolving Complex of Photosystem II

Maria Drosou,[a,b,*] Dimitrios A. Pantazis[a,*]

[a] Max-Planck-Institut für Kohlenforschung Kaiser-Wilhelm-Platz 1, 45470, Mülheim an der Ruhr, Germany

[b] Inorganic Chemistry Laboratory, National and Kapodistrian University of Athens, Panepistimiopolis, Zografou 15771, Greece

E-mail: drosou@kofo.mpg.de, dimitrios.pantazis@kofo.mpg.de

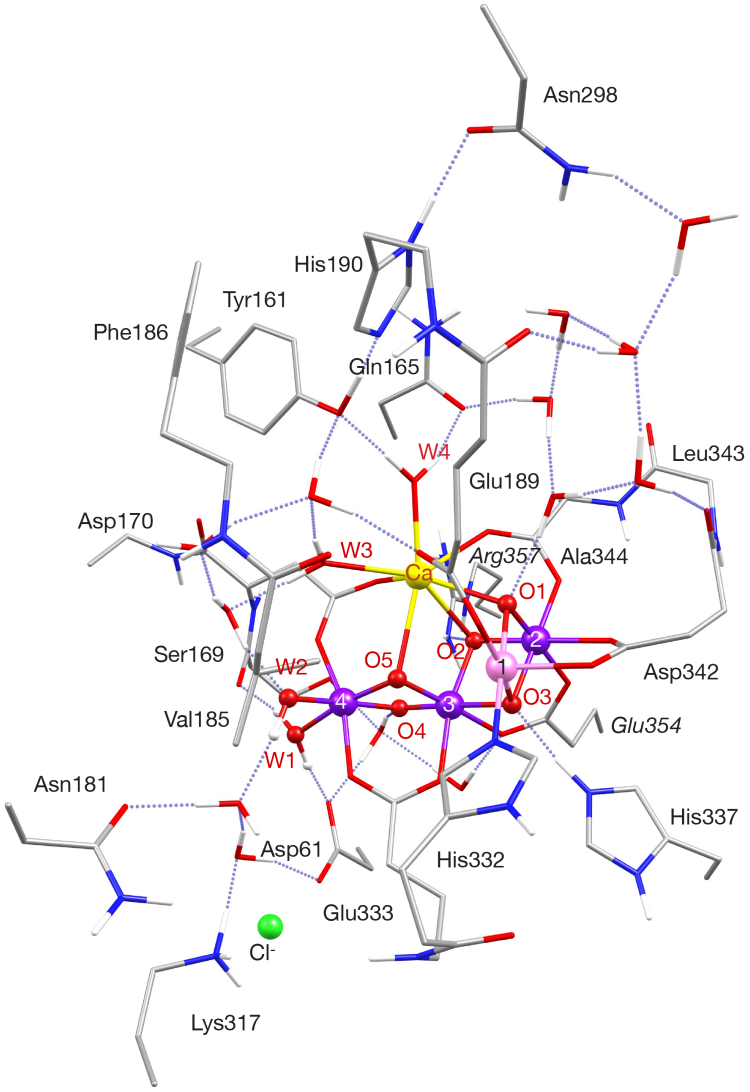

Figure S1. Complete computational model for the S_2 state of the OEC. Mn(III) ions are indicated in pink, Mn(IV) in dark purple, Ca in yellow, N in blue, O in red and Cl in green. Hydrogen atoms connected to carbon atoms are omitted for clarity. All amino-acid residues belong to the D1 subunit, except from Arg357 and Glu354 (shown in *italics*), which belong to the CP43 subunit.

Table S1. Structural parameters of BP86/ZORA-TZVP optimized S_2-state structures with various NH_3 binding sites. The corresponding core structures are shown in Figures 4–6 of the manuscript.

	Mn1-Mn2	Mn1-Mn3	Mn2-Mn3	Mn3-Mn4	Mn[a]-NHx	Mn1-N(His)	Mn3-O5	Mn[b]-O5	Mn4-O(W1)	Mn4-O(W2)
S_2	2.765	3.386	2.814	2.768	-	2.022	1.846	1.881	2.032	1.862
S_2^H	2.772	3.373	2.800	2.755	-	2.016	1.860	1.861	2.008	2.039
A1	2.751	3.618	2.901	3.023	1.932	2.041	-	1.803	1.957	2.231
A2	2.797	3.565	2.833	2.866	1.885	2.041	-	2.139	2.002	2.066
A3	2.765	3.362	2.850	2.758	1.881	2.021	-	-	2.046	2.068
A4	2.757	3.412	2.830	2.903	2.005	2.021	-	-	1.968	1.850
A5	2.797	3.426	2.825	2.714	1.815	2.056	-	-	2.112	2.078
A6	2.764	3.382	2.813	2.804	1.924	2.031	-	-	2.071	1.867
A7	2.770	3.374	2.798	2.793	1.914	2.024	-	-	2.044	2.039
A8	2.770	3.271	2.835	2.695	1.879	2.033	-	-	2.198	1.890
A9	2.771	3.300	2.812	2.683	1.843	2.029	-	-	2.161	2.069
A10	2.768	3.387	2.809	2.892	2.009	2.009	-	-	1.946	2.015
B1	2.766	3.350	2.810	2.771	2.061	2.025	1.832	1.917	-	1.869
B2	2.742	2.923	2.782	3.112	2.182	2.055	1.888	1.884	-	1.866
B3	2.773	3.342	2.799	2.759	2.059	2.018	1.848	1.891	-	2.039
B4	2.745	2.907	2.770	3.150	2.167	2.050	1.880	1.883	-	2.035
C1	2.766	3.360	2.807	2.773	2.056	2.025	1.812	1.985	1.814	-
C2	2.769	3.391	2.801	2.748	2.060	2.017	1.862	1.859	1.997	-
C3	2.745	2.909	2.768	3.118	2.062	2.052	1.884	1.886	2.114	-
D1	2.748	3.118	2.835	3.205	2.077	2.057	2.254	1.774	2.155	1.786
D2	2.787	3.595	2.854	2.882	2.050	2.062	1.858	1.857	-	2.280
D3	2.747	3.147	2.843	3.276	2.004	2.057	2.263	1.785	1.895	1.958
D4	2.786	3.533	2.826	2.830	2.043	2.064	1.852	1.879	-	1.871
D5	2.777	3.154	2.783	3.260	1.985	2.025	1.898	2.208	2.091	1.888
D6	2.749	3.193	2.831	3.232	2.030	2.051	2.210	1.873	2.112	1.861
D7	2.757	3.755	2.917	2.959	2.014	2.043	1.958	1.915	-	2.072
D8	2.747	3.096	2.819	3.287	1.981	2.056	2.230	1.779	1.940	2.125
E1	2.798	3.427	2.829	2.805	2.415	2.082	1.789	1.953	1.834	1.857
E2	2.857	3.548	2.842	2.803	2.018	2.359	1.859	1.848	2.001	1.872
E3	2.804	3.410	2.813	2.762	2.430	2.065	1.847	1.827	1.995	2.062
E4	2.783	3.572	2.853	2.789	1.980	2.066	1.843	1.875	1.975	2.072

[a]Mn4 ion in binding modes A–D and Mn1 in mode E.

[b]Mn1 ion for closed-cubane structures and Mn4 ion for open-cubane structures.

Table S2. Calculated Mulliken Mn spin populations for the optimized S_2 and S_2-NH_3 models calculated with broken-symmetry (BS) TPSSh using the lowest energy BS determinant. Very similar spin populations are computed with BP86 and with TPSSh using the high-spin determinant.

	Mn1	Mn2	Mn3	Mn4
S_2	3.90	-2.96	-2.90	2.91
S_2^H	3.89	-2.96	-2.93	2.92
A1	2.96	2.99	2.79	-3.99
A2	-3.89	2.94	3.12	3.10
A3	-3.88	2.97	2.99	3.02
A4	3.88	-2.98	-2.89	2.97
A5	3.92	-2.94	-2.84	2.73
A6	-3.90	2.95	2.99	3.02
A7	-3.88	2.95	3.03	3.03
A8	3.91	-2.92	-2.75	2.79
A9	3.90	-2.94	-2.80	2.70
A10	3.86	-2.97	-2.93	2.98
B1	3.94	-2.97	-2.92	2.96
B2	3.03	2.93	2.96	3.84
B3	3.89	-2.96	-2.93	2.95
B4	2.99	2.93	2.99	3.90
C1	3.90	-2.94	-2.89	2.84
C2	3.89	-2.96	-2.92	2.94
C3	2.97	2.93	2.87	-3.90
D1	2.87	2.91	-3.84	2.79
D2	2.91	2.96	2.78	-3.95
D3	2.88	2.90	-3.83	2.92
D4	3.90	-2.93	-2.93	2.95
D5	3.88	-2.90	2.95	-2.89
D6	2.98	2.90	-3.84	2.86
D7	2.99	2.99	3.89	-2.81
D8	2.88	2.91	-3.82	2.77
E1	3.92	-2.93	-2.83	2.87
E2	3.90	-2.88	-2.93	2.91
E3	3.92	-2.95	-2.93	2.90
E4	2.97	-2.96	-2.81	3.91

Table S3. Relative energies (kcal mol^{-1}) of BP86 optimized S_2-state structures with various NH_3 binding sites calculated with BP86, TPSSh using the high-spin determinant and broken-symmetry (BS) TPSSh using the lowest energy BS determinant.

(O,H)		BP86	TPSSh	BS-TPSSh
(2,4)	**A6**	15.0	19.6	19.4
	A9	24.4	26.7	25.5
	B1	0.0	0.0	0.0
	B2	8.3	10.4	11.1
	C1	1.3	6.5	6.4
(2,5)	**A4**	32.5	39.9	39.9
	A7	20.0	21.9	21.7
	B3	3.5	1.3	1.4
	B4	8.6	5.2	6.0
	C2	0.0	0.0	0.0
	C3	5.1	4.6	5.1
(3,6)	**A5**	23.0	27.3	26.2
	D1	9.8	12.5	12.2
	D2	0.0	0.0	0.0
	D3	10.3	13.8	12.7
	D4	7.0	5.9	5.1
	E2	15.1	20.4	19.6
(3,7)	**A1**	24.1	26.8	26.4
	A2	33.2	36.9	36.4
	A3	34.6	45.0	45.5
	D5	10.9	13.4	13.7
	D6	3.9	8.0	8.2
	D7	0.0	0.0	0.0
	D8	9.1	14.1	12.8
	E3	5.0	7.5	6.7
	E4	9.9	16.1	13.8

Table S4. Calculated effective/projected axial ($A_{\|}$) and equatorial ($A_{\perp}$) ^{55}Mn hyperfine coupling constants, as well as isotropic ($a_{\|}$) and anisotropic ($a_{\perp}$) on-site hyperfine values and spin projection coefficients ρ_i for each Mn ion, Mn_i, of the S_2-NH_3 and the S_2-state models in the low-spin ($S = 1/2$) configuration.

		Mn1(III)	Mn2(IV)	Mn3(IV)	Mn4(IV)
A4	$A_{BS,x}$ [a]	-179	402	369	-438
	$A_{BS,y}$	-468	415	377	-469
	$A_{BS,z}$	-534	440	437	-498
	$A_{\|}$ [b]	-85	-199	-240	-419
	$A_{\perp}$ [c]	-239	-185	-205	-463
	ρ_i	1.07	-0.76	-0.92	1.61
	α_{iso} [d]	-175	249	234	-278
	α_{aniso} [e]	-143	-19	-38	-27
A5	$A_{BS,x}$	-265	397	404	-450
	$A_{BS,y}$	-579	407	460	-524
	$A_{BS,z}$	-605	447	471	-542
	$A_{\|}$	-229	-265	-173	-210
	$A_{\perp}$	-510	-238	-199	-248
	ρ_i	1.94	-1.00	-0.72	0.78
	α_{iso}	-215	247	264	-300
	α_{aniso}	-145	-26	37	-49
A8	$A_{BS,x}$	-154	418	398	-427
	$A_{BS,y}$	-454	425	430	-525
	$A_{BS,z}$	-491	461	444	-539
	$A_{\|}$	-133	-273	-201	-209
	$A_{\perp}$	-407	-250	-187	-260
	ρ_i	1.94	-1.00	-0.76	0.82
	α_{iso}	-163	258	252	-295
	α_{aniso}	-142	-23	-18	-62
A9	$A_{BS,x}$	-172	407	404	-446
	$A_{BS,y}$	-464	417	463	-525
	$A_{BS,z}$	-522	452	473	-549
	$A_{\|}$	-151	-266	-156	-177
	$A_{\perp}$	-433	-242	-181	-213
	ρ_i	1.97	-0.99	-0.65	0.67
	α_{iso}	-172	253	265	-301
	α_{aniso}	-143	-24	38	-54
A10	$A_{BS,x}$	-211	393	389	-429

	$A_{BS,y}$	-476	404	400	-470
	$A_{BS,z}$	-579	431	446	-495
	$A_{\parallel}$	-96	-210	-220	-416
	$A_{\perp}$	-238	-194	-194	-468
	ρ_i	1.01	-0.82	-0.83	1.63
	α_{iso}	-188	243	244	-276
	α_{aniso}	-141	-19	-31	-32
B1	$A_{BS,x}$	-167	404	369	-426
	$A_{BS,y}$	-463	416	384	-466
	$A_{BS,z}$	-521	447	421	-503
	$A_{\parallel}$	-135	-263	-221	-315
	$A_{\perp}$	-398	-241	-198	-279
	ρ_i	1.82	-0.99	-0.89	1.06
	α_{iso}	-171	251	232	-276
	α_{aniso}	-144	-22	-27	-35
B3	$A_{BS,x}$	-176	392	390	-424
	$A_{BS,y}$	-466	405	417	-471
	$A_{BS,z}$	-535	437	449	-492
	$A_{\parallel}$	-131	-251	-261	-320
	$A_{\perp}$	-373	-229	-234	-364
	ρ_i	1.68	-0.97	-0.98	-0.98
	α_{iso}	-174	244	248	-274
	α_{aniso}	-144	-23	-27	-34
C1	$A_{BS,x}$	-167	406	369	-450
	$A_{BS,y}$	-461	417	378	-461
	$A_{BS,z}$	-521	450	407	-498
	$A_{\parallel}$	-147	-262	-147	-179
	$A_{\perp}$	-434	-240	-135	-164
	ρ_i	1.99	-0.98	-0.61	0.61
	α_{iso}	-170	252	228	-279
	α_{aniso}	-144	-23	-20	25
C2	$A_{BS,x}$	-175	397	390	-442
	$A_{BS,y}$	-463	410	416	-476
	$A_{BS,z}$	-533	441	449	-483
	$A_{\parallel}$	-123	-247	-264	-354
	$A_{\perp}$	-352	-226	-238	-384
	ρ_i	1.59	-0.94	-0.99	1.35
	α_{iso}	-174	247	248	-277

	α_{aniso}	-144	-23	-27	-22
D4	$A_{\text{BS},x}$	-368	386	349	-419
	$A_{\text{BS},y}$	-679	399	375	-453
	$A_{\text{BS},z}$	-730	437	426	-500
	$A_{\parallel}$	-204	-196	-252	-447
	$A_{\perp}$	-391	-177	-214	-390
	ρ_i	1.25	-0.76	-1.00	1.51
	α_{iso}	-264	242	228	-271
	α_{aniso}	-150	-26	-38	38
D5	$A_{\text{BS},x}$	-311	471	-430	397
	$A_{\text{BS},y}$	-589	481	-447	422
	$A_{\text{BS},z}$	-675	503	-509	464
	$A_{\parallel}$	-203	-231	-376	-258
	$A_{\perp}$	-412	-219	-324	-228
	ρ_i	1.47	-0.77	1.25	-0.94
	α_{iso}	-234	288	-274	254
	α_{aniso}	-143	-16	42	-33
E1	$A_{\text{BS},x}$	-291	408	355	-475
	$A_{\text{BS},y}$	-603	417	362	-484
	$A_{\text{BS},z}$	-624	452	392	-503
	$A_{\parallel}$	-257	-267	-106	-139
	$A_{\perp}$	-542	-244	-97	-132
	ρ_i	1.99	-1.00	-0.45	0.46
	α_{iso}	-225	252	219	-289
	α_{aniso}	-143	-24	-20	14
E2	$A_{\text{BS},x}$	-315	371	362	-437
	$A_{\text{BS},y}$	-556	394	389	-473
	$A_{\text{BS},z}$	-679	428	436	-512
	$A_{\parallel}$	-207	-218	-256	-417
	$A_{\perp}$	-405	-195	-220	-370
	ρ_i	1.47	-0.86	-0.99	1.37
	α_{iso}	-230	236	235	-281
	α_{aniso}	-135	-27	-36	34
E3	$A_{\text{BS},x}$	-287	388	386	-439
	$A_{\text{BS},y}$	-601	399	419	-481
	$A_{\text{BS},z}$	-622	432	452	-493
	$A_{\parallel}$	-197	-228	-224	-343

	$A_\perp$	-421	-208	-252	-381
	ρ_i	1.55	-0.89	-0.98	1.32
	α_{iso}	-224	241	249	-280
	α_{aniso}	-145	-23	29	-28
S_2	$A_{BS,x}$	-165	405	366	-437
	$A_{BS,y}$	-459	418	385	-479
	$A_{BS,z}$	-519	449	423	-515
	$A_\parallel$	-131	-261	-227	-287
	$A_\perp$	-387	-239	-202	326
	ρ_i	1.78	-0.98	-0.91	1.11
	α_{iso}	-170	251	232	-283
	α_{aniso}	-144	-22	-28	-35
S_2^H	$A_{BS,x}$	-175	393	386	-443
	$A_{BS,y}$	-463	407	415	-485
	$A_{BS,z}$	-534	438	447	-494
	$A_\parallel$	-127	-249	-262	-344
	$A_\perp$	-363	-227	-235	-380
	ρ_i	1.64	-0.96	-0.99	1.31
	α_{iso}	-174	245	247	-281
	α_{aniso}	-144	-22	-28	-27

[a] $A_{BS,x}$, $A_{BS,y}$, $A_{BS,z}$ are the components of the hyperfine coupling tensor computed from the BS calculation and following the convention $|A_{BS,z}| > |A_{BS,y}| > |A_{BS,x}|$. The effective (observable) HFC components $-A_x$, A_y, A_z- of Mn_i are derived from: $A_x = A_{BS,x} \cdot \frac{\langle S_z \rangle_{BS}}{S_i} \cdot \rho_i \cdot 1.78$, where S_i is the site spin of Mn_i [2 for Mn(III) and 3/2 for Mn(IV)], $\langle S_z \rangle_{BS}$ the total M_S of the BS wavefunction (1/2 in all models), ρ_i the spin projection coefficient of Mn_i,[1] and 1.78 is a scaling factor used specifically for comparing the computed ^{55}Mn hyperfine coupling constants with experimental results (see also Computational Details section in the main text).

[b] $A_\parallel$ is defined as the component of the effective HFC components with the largest difference to $A_{iso} = (A_x + A_y + A_z)/3$ (Table 2), and $A_\perp$ the average of those components with the smallest difference to A_{iso}.

[c] The on-site hyperfine values $-a_x$, a_y, a_z- of Mn_i are derived from: $a_x = A_{BS,x} \cdot \frac{\langle S_z \rangle_{BS}}{S_i} \cdot 1.78$, and $\alpha_{iso} = (\alpha_x + \alpha_y + \alpha_z)/3$.

[b] α_{aniso} is defined as $\alpha_{aniso} = \alpha_\perp - \alpha_\parallel$, where $\alpha_\parallel$ the on-site HFC component with the largest difference to α_{iso} and $\alpha_\perp$ the average of those components with the smallest difference to a_{iso}.

Table S5. Calculated effective/projected ^{14}N hyperfine and NQI tensors (in MHz) for the electron–nuclear couplings of the bound NH_x-N and of the His332 imino-N, and ^{17}O hyperfine tensors (in MHz) of the terminal W1 and W2 ligands and the bridging O5 ligand for the S_2-NH_3 and the S_2-state models in the low-spin ($S = 1/2$) configuration.

		^{14}N			^{17}O	
		NH_3	His332	O5	W2	W1
A4	$A_{BS,x}$ [a]	3.64	-10.76		15.04	2.18
	$A_{BS,y}$	8.12	-13.25		-15.40	-3.04
	$A_{BS,z}$	9.96	-14.26		-62.54	-15.96
	$\lvert A_{iso}\rvert$ [b]	3.06	3.42	-	16.66	3.80
	A_{dip} [c]	0.76	0.27	-	-8.48	-2.20
	A_η [d]	0.51	0.51	-	0.01	0.10
	$\lvert e^2Qq/h\rvert$	1.44	1.96			
	η	0.81	0.85			
A5	$A_{BS,x}$	6.64	-2.38		0.97	-0.18
	$A_{BS,y}$	14.86	-6.17		-1.25	-1.76
	$A_{BS,z}$	-16.96	-6.89		-4.23	-6.31
	$\lvert A_{iso}\rvert$	6.43	2.49	-	0.56	0.72
	A_{dip}	1.55	0.67	-	-0.27	-0.47
	A_η	0.34	0.26	-	0.13	0.45
	$\lvert e^2Qq/h\rvert$	0.8	2.23			
	η	0.88	0.60			
A8	$A_{BS,x}$	5.66	-8.10		1.09	-1.93
	$A_{BS,y}$	-9.59	-11.39		-1.22	-4.41
	$A_{BS,z}$	25.74	-12.65		-39.93	-6.27
	$\lvert A_{iso}\rvert$	3.61	5.18	-	3.87	1.16
	A_{dip}	-1.60	0.63	-	-3.55	0.31
	A_η	0.33	0.48	-	0.01	0.81
	$\lvert e^2Qq/h\rvert$	0.87	2.23			
	η	0.97	0.50			
A9	$A_{BS,x}$	-12.35	-8.82		-0.13	-1.71
	$A_{BS,y}$	12.91	-11.89		1.81	-3.81
	$A_{BS,z}$	23.75	-13.04		-3.97	-6.42
	$\lvert A_{iso}\rvert$	3.59	5.55	-	0.44	0.89
	A_{dip}	-0.81	0.60	-	-0.22	-0.27
	A_η	0.08	0.47	-	0.84	0.86
	$\lvert e^2Qq/h\rvert$	0.62	2.16			
	η	0.96	0.56			

A10	$A_{BS,x}$	1.53	-11.81		0.45	-2.50
	$A_{BS,y}$	6.51	-14.00		1.05	-30.93
	$A_{BS,z}$	9.12	-15.04		-1.49	-30.93
	$\|A_{iso}\|$	2.35	3.45	-	0.54	8.18
	A_{dip}	0.86	0.23	-	0.15	-4.33
	A_η	0.62	0.57	-	0.82	0.57
	$\|e^2Qq/h\|$	1.33	1.86			
	η	0.80	0.82			
B1	$A_{BS,x}$	-7.73	-9.65	6.62	10.71	
	$A_{BS,y}$	-7.90	-12.54	28.15	-11.25	
	$A_{BS,z}$	-10.23	-13.69	-40.78	-52.28	
	$\|A_{iso}\|$	3.03	5.44	8.14	4.66	-
	A_{dip}	-0.28	0.52	3.00	-2.47	-
	A_η	0.10	0.50	0.68	0.24	-
	$\|e^2Qq/h\|$	1.27	2.09			
	η	0.77	0.71			
B3	$A_{BS,x}$	-7.54	-10.34	-10.28	1.41	
	$A_{BS,y}$	-7.57	-12.97	28.88	2.46	
	$A_{BS,z}$	-9.87	-14.04	-47.07	-6.01	
	$\|A_{iso}\|$	3.53	5.21	10.79	1.40	-
	A_{dip}	-0.33	0.44	3.46	-0.58	-
	A_η	0.02	0.51	0.99	0.39	-
	$\|e^2Qq/h\|$	1.29	2.00			
	η	0.91	0.79			
C1	$A_{BS,x}$	-5.88	-9.46	20.12	17.00	
	$A_{BS,y}$	-6.10	-12.43	26.68	-22.23	
	$A_{BS,z}$	-6.21	-13.54	-40.98	-91.64	
	$\|A_{iso}\|$	1.23	5.87	11.87	-	8.82
	A_{dip}	0.02	0.58	-2.38	-	-4.85
	A_η	0.61	0.47	0.56	-	0.11
	$\|e^2Qq/h\|$	1.84	2.12			
	η	0.30	0.70			
C2	$A_{BS,x}$	-7.78	-10.31	-17.19	0.98	
	$A_{BS,y}$	-7.97	-12.96	32.91	-4.03	
	$A_{BS,z}$	-9.03	-14.01	-43.88	-17.53	
	$\|A_{iso}\|$	3.71	4.93	12.23	-	3.38
	A_{dip}	-0.17	0.42	2.76	-	-2.25

	A_η	0.25	0.50	0.78	-	0.30
	$\lvert e^2Qq/h \rvert$	1.68	2.00			
	η	0.34	0.79			
D4	$A_{BS,x}$	-8.17	-0.24	4.85	10.47	-41.35
	$A_{BS,y}$	-8.41	-4.11	-26.54	-11.25	-44.09
	$A_{BS,z}$	-11.09	-4.73	27.70	-51.66	-76.52
	$\lvert A_{iso} \rvert$	4.64	0.95	8.22	12.29	16.84
	A_{dip}	-0.47	0.43	3.10	-6.84	-3.51
	A_η	0.12	0.22	0.08	0.03	0.12
	$\lvert e^2Qq/h \rvert$	1.23	2.23			
	η	0.90	0.59			
D5	$A_{BS,x}$	5.21	-7.28	-50.40	1.48	2.27
	$A_{BS,y}$	5.54	-10.76	-94.61	-1.95	-10.72
	$A_{BS,z}$	8.33	-11.44	-115.06	-5.70	21.23
	$\lvert A_{iso} \rvert$	1.99	3.60	33.89	0.95	3.56
	A_{dip}	-0.31	0.47	7.09	-0.41	-1.54
	A_η	0.17	0.27	0.56	0.18	0.86
	$\lvert e^2Qq/h \rvert$	0.98	2.10			
	η	0.73	0.71			
E1	$A_{BS,x}$	23.73	2.06	27.36	10.69	17.70
	$A_{BS,y}$	23.82	-2.25	-30.07	-25.77	-20.79
	$A_{BS,z}$	35.03	-2.85	36.09	-67.39	-67.36
	$\lvert A_{iso} \rvert$	13.68	1.18	4.77	5.35	5.46
	A_{dip}	-1.86	-0.11	-0.38	-2.53	-2.48
	A_η	0.01	0.40	0.55	0.46	0.10
	$\lvert e^2Qq/h \rvert$	2.89	2.48			
	η	0.31	0.47			
E2	$A_{BS,x}$	-5.21	25.31	0.57	10.66	3.46
	$A_{BS,y}$	-7.26	25.82	-26.76	-10.80	-5.85
	$A_{BS,z}$	-8.22	32.01	38.26	-51.07	6.26
	$\lvert A_{iso} \rvert$	3.15	10.21	8.60	11.06	2.37
	A_{dip}	0.39	-0.79	4.19	-5.51	0.47
	A_η	0.57	0.12	0.54	0.01	0.20
	$\lvert e^2Qq/h \rvert$	1.73	3.37			
	η	0.72	0.18			
E3	$A_{BS,x}$	23.85	0.30	-14.51	-1.35	-1.55
	$A_{BS,y}$	23.94	-3.69	-36.67	-2.54	2.29

	$A_{BS,z}$	34.10	-4.24	39.40	-7.89	-13.57
	$\|A_{iso}\|$	10.56	1.06	11.54	1.73	2.55
	A_{dip}	-1.32	0.47	3.00	-0.87	-1.70
	A_η	0.01	0.22	0.17	0.30	0.10
	$\|e^2Qq/h\|$	2.94	2.27			
	η	0.19	0.61			
S_2	$A_{BS,x}$		-9.80	2.36	9.93	1.37
	$A_{BS,y}$		-12.66	36.65	-10.16	3.71
	$A_{BS,z}$		-13.81	-37.39	-56.84	-5.09
	$\|A_{iso}\|$		5.38	8.53	9.45	1.25
	A_{dip}		0.51	3.87	-5.75	0.37
	A_η		0.50	0.03	0.01	0.68
	$\|e^2Qq/h\|$		2.08			
	η		0.72			
S_2^H	$A_{BS,x}$		-10.48	-14.56	-0.17	1.34
	$A_{BS,y}$		-13.09	35.52	0.75	-2.75
	$A_{BS,z}$		-14.15	-44.25	-7.63	-13.26
	$\|A_{iso}\|$		5.14	12.02	1.24	2.52
	A_{dip}		0.43	3.23	-1.04	-2.27
	A_η		0.51	0.52	0.12	0.14
	$\|e^2Qq/h\|$		1.99			
	η		0.80			

[a] $A_{BS,x}$, $A_{BS,y}$, $A_{BS,z}$ are the components of the hyperfine coupling tensor computed from the BS calculation and they follow the convention $|A_{BS,z}| > |A_{BS,y}| > |A_{BS,x}|$. The effective (observable) HFC components $-A_x$, A_y, A_z– of ^{14}N or ^{17}O ligand to Mn_i are derived from: $A_x = A_{BS,x} \cdot \frac{\langle S_z \rangle_{BS}}{S_i} \cdot \rho_i$, where S_i is the site spin of Mn_i [2 for Mn(III) and 3/2 for Mn(IV)], $\langle S_z \rangle_{BS}$ the total M_S of the BS wavefunction (1/2 in all models), and ρ_i the spin projection coefficient of Mn_i. For a bridging ligand coordinated to Mn_j and Mn_k, such as NH_x in models A and O5, the effective HFC components are derived from $A_x = \frac{A_{BS,x}}{2} \cdot (\frac{\langle S_z \rangle_{BS}}{S_j} \cdot |\rho_j| + \frac{\langle S_z \rangle_{BS}}{S_k} \cdot |\rho_k|)$, where S_j and ρ_j are the site spin and the spin projection coefficient, respectively, of Mn_j.[1-3]

[b] $|A_{iso}|$ is defined as the average of the principal components of the effective hyperfine tensor: $|A_{iso}| = (|A_x| + |A_y| + |A_z|)/3$.

[c] A_{dip} is defined as $A_{dip} = (T_1 + T_2)/2 = -T_3/2$, where T_1, T_2, and T_3 represent the three principal components of the hyperfine tensors minus A_{iso}, i.e. $|A_x| - |A_{iso}|$, $|A_y| - |A_{iso}|$, and $|A_z| - |A_{iso}|$, respectively, and are labeled such that $|T_1| \leq |T_2| \leq |T_3|$. [d] The rhombicity is defined as $A_\eta = (T_1 - T_2)/T_3$, respectively.

Table S6. Electron affinity (EA) differences between S_2-NH_3 and the S_2-state models, i.e. ΔE = EA(S_2) – EA(S_2-NH_3). Comparisons are made between structures having the same charge, thus models **A5**, **B1**, **C1**, **D4**, and **E2** are compared with $\mathbf{S_2}$ and models **A4**, **A9**, **B3**, **C2**, **D5**, and **E3** are compared with $\mathbf{S_2^H}$.

		ΔE (kcal mol^{-1})
S_2	**A5**	8.73
	B1	2.19
	C1	4.43
	D4	2.39
	E2	0.68
S_2^H	**A4**	0.34
	A9	9.87
	B3	1.57
	C2	1.97
	D5	3.33
	E3	2.90

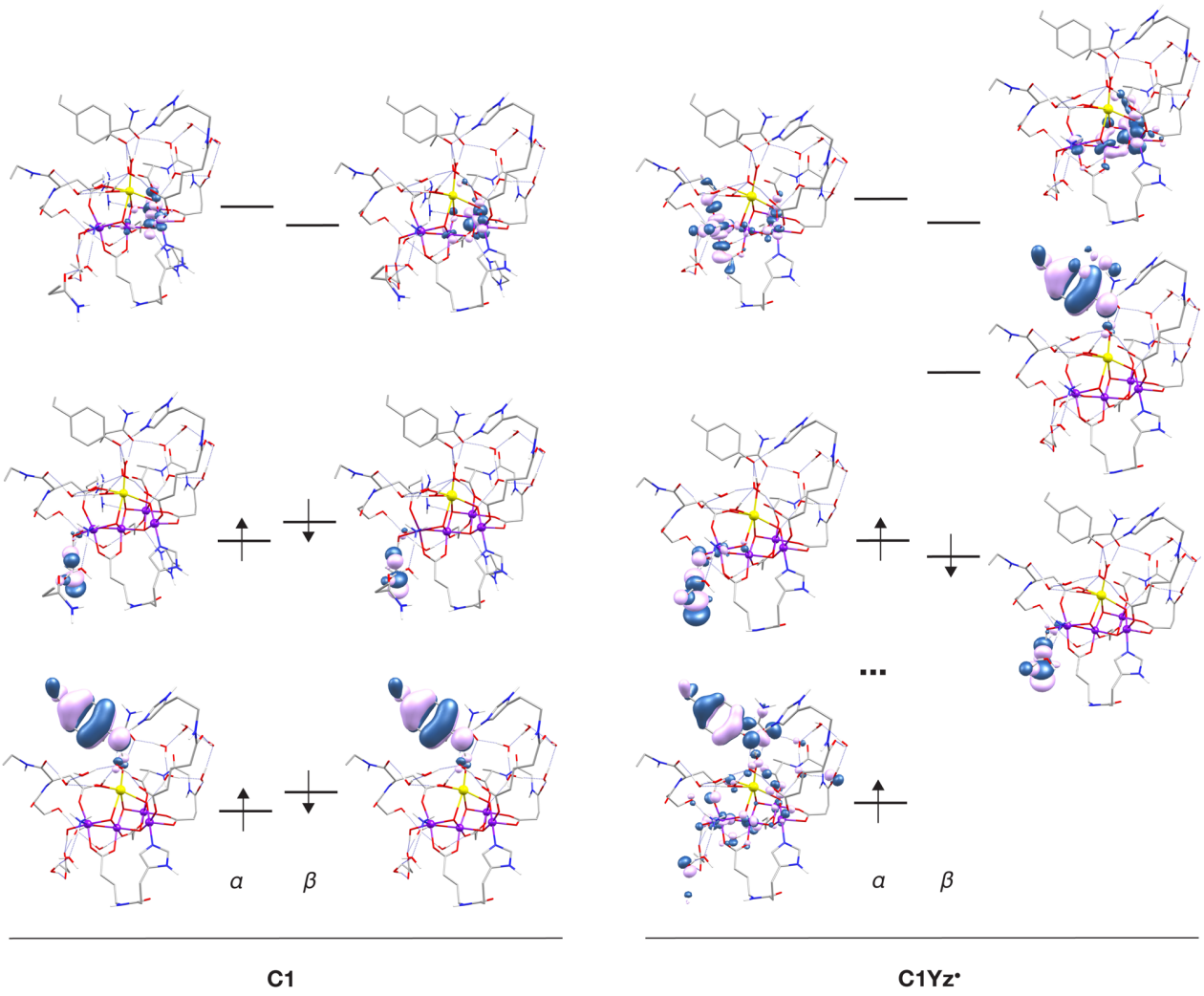

Figure S2. Frontier orbitals of model **C1** of the ammonia-bound S_2 state of the OEC (left) and of the oxidized $\mathbf{C1Y_z^{\bullet}}$ (right); hydrogen atoms are omitted for clarity.

Table S7. Comparison of calculated ^{55}Mn HFCs (MHz) for the model in which ammonia binds on the W1 position (**B1**) between this work, Schraut and Kaupp,[4] and Lohmiller et al.[5]

	A_1	A_2	A_3	A_4	A_1/A_2	A_2/A_3	A_3/A_4
B1	311 [1]	291 [4]	248 [2]	206 [3]	1.07	1.17	1.21
Ref 4	295 [1]	192 [2]	160 [4]	120 [3]	1.54	1.20	1.33
Ref 5	244 [1]	227 [4]	215 [2]	166 [3]	1.07	1.06	1.30

Table S8. Comparison of calculated ^{14}N HFCs and NQI asymmetry (η) for **B1** between this work, Schraut and Kaupp,[4] and Lohmiller et al.[5]

	NH_3		His332	
	$\lvert A_{iso}\rvert$	η	$\lvert A_{iso}\rvert$	η
B1	3.03	0.77	5.44	0.71
Ref 4	3.39	0.35	5.67	0.94
Ref 5	2.68	0.87	6.10	0.88

Orca Input files

Broken-Symmetry:

```
! UKS TPSSh RIJCOSX ZORA ZORA-TZVP SARC/J
! Grid5 GridX7 NoFinalGrid TightSCF moread

%pal nprocs 10 end
%maxcore 3000

%moinp "filename.gbw"

%basis newgto C "ZORA-SVP" end
       newgto H "ZORA-SVP" end
end

%method intacc 6.0 end

%scf maxiter 200
     shift shift 0.10 erroff 0.1 end
     FlipSpin 1,2 FinalMs 0.5
end


*xyzfile 1 14 filename.xyz
```

Mn hyperfine coupling tensors:

```
! UKS TPSSh RIJCOSX ZORA ZORA-def2-TZVP(-f) SARC/J
! Grid5 GridX7 NoFinalGrid Slowconv TightSCF moread

%pal nprocs 10 end
%maxcore 15000

%moinp "filename.gbw"

%basis newgto C "ZORA-def2-SVP" end
       newgto H "ZORA-def2-SVP" end
       newgto Mn
 S 1
   1 4331015.6489100000      1.0000000000
 S 1
   1 1732406.2595600000      1.0000000000
 S 1
   1  692962.5038250000      1.0000000000
 S 1
   1  277185.0015300000      1.0000000000
 S 1
   1   41550.7698900000      1.0000000000
 S 1
   1    9455.9700152000      1.0000000000
 S 1
   1    2676.5206482000      1.0000000000
 S 1
   1     871.4668753000      1.0000000000
 S 1
   1     312.9830642000      1.0000000000
 S 1
   1     121.4445405100      1.0000000000
 S 1
   1      47.9225988300      1.0000000000
 S 1
   1     303.6672316300      1.0000000000
```

```
 S 1
   1      93.8814031900      1.0000000000
 S 1
   1      14.8794212100      1.0000000000
 S 1
   1       6.2865200700     -1.0000000000
 S 1
   1       9.4858591300      1.0000000000
 S 1
   1       1.5698706200      1.0000000000
 S 1
   1       0.6590321400     -1.0000000000
 S 1
   1       0.1068629200     -1.0000000000
 S 1
   1       0.0392674400     -1.0000000000
 P 6
   1    1444.7978182000      0.0032493630
   2     342.0655119700      0.0237346473
   3     109.5840089100      0.1067232634
   4      40.7479881700      0.3007617717
   5      16.1886265700      0.4790147038
   6       6.5484506000      0.2708283465
 P 1
   1      25.3570864400     -1.0000000000
 P 1
   1       3.4830168800      1.0000000000
 P 1
   1       1.3858800900      1.0000000000
 P 1
   1       0.5255509500     -1.0000000000
 P 1
   1       0.1276500000      1.0000000000
 D 4
   1      56.5631891200      0.0192444440
   2      16.2787347100      0.1161060412
   3       5.6964273900      0.3706567953
   4       2.1411147900      0.6570040408
 D 1
   1       0.7829180200      1.0000000000
 D 1
   1       0.2595231100      1.0000000000
 D 1
   1       0.0860000000      1.0000000000
 F 1
   1       1.3260000000      1.0000000000
 end
end

%method intacc 6.0
        SpecialGridAtoms 25
        SpecialGridIntAcc 11
end

%rel picturechange true end

%scf maxiter 200
     shift shift 0.10 erroff 0.1 end
     CNVSOSCF true SOSCFstart 0.001
end

*xyzfile 1 2 filename.xyz

%eprnmr   nuclei = all Mn { aiso, adip, aorb }
end
```

N and O hyperfine coupling tensors:

```
! UKS TPSSh RIJCOSX ZORA ZORA-def2-TZVP(-f) SARC/J
! Grid5 GridX7 NoFinalGrid Slowconv TightSCF moread

%pal nprocs 10 end
%maxcore 15000

%moinp "filename.gbw"

%basis
 NewGTO N
 S 1
   1   308293.7601093750      1.0000000000
 S 1
   1   123317.5040437500      1.0000000000
 S 1
   1    49327.0016175000      1.0000000000
 S 1
   1    19730.8006470000      1.0000000000
 S 1
   1     2957.8958745000      1.0000000000
 S 1
   1      673.2213359500      1.0000000000
 S 1
   1      190.6824949400      1.0000000000
 S 1
   1       62.2954419000      1.0000000000
 S 1
   1       22.6541611800      1.0000000000
 S 1
   1        8.9791477400      1.0000000000
 S 1
   1        3.6863002400      1.0000000000
 S 1
   1        0.8466007700      1.0000000000
 S 1
   1        0.3364713400      1.0000000000
 S 1
   1        0.1364765400      1.0000000000
 P 4
   1       49.2003805100      0.0115131336
   2       11.3467905400      0.0785386070
   3        3.4273972400      0.3081978103
   4        1.1785525100      0.7201896814
 P 1
   1        0.4164220500      1.0000000000
 P 1
   1        0.1426082600      1.0000000000
 D 1
   1        1.6540000000      1.0000000000
 D 1
   1        0.4690000000      1.0000000000
 end
NewGTO O
 S 1
   1   422380.9786093750      1.0000000000
 S 1
   1   168952.3914437500      1.0000000000
 S 1
   1    67580.9565775000      1.0000000000
 S 1
   1    27032.3826310000      1.0000000000
 S 1
```

```
   1     4052.3871392000      1.0000000000
 S 1
   1      922.3272271000      1.0000000000
 S 1
   1      261.2407098900      1.0000000000
 S 1
   1       85.3546413500      1.0000000000
 S 1
   1       31.0350352400      1.0000000000
 S 1
   1       12.2608607300      1.0000000000
 S 1
   1        4.9987076000      1.0000000000
 S 1
   1        1.1703108200      1.0000000000
 S 1
   1        0.4647474100      1.0000000000
 S 1
   1        0.1850453600      1.0000000000
 P 4
   1       63.2749548000      0.0121096626
   2       14.6270493800      0.0831734399
   3        4.4501223500      0.3200012219
   4        1.5275799600      0.7069790865
 P 1
   1        0.5293511800      1.0000000000
 P 1
   1        0.1747842100      1.0000000000
 D 1
   1        2.3140000000      1.0000000000
 D 1
   1        0.6450000000      1.0000000000
 end
end

%method intacc 6.0
        SpecialGridAtoms 8,7
        SpecialGridIntAcc 9,9
end

%rel
     SOCFlags 1,3,3,1
     picturechange true
end

%scf maxiter 200
     shift shift 0.10 erroff 0.1 end
     CNVSOSCF true SOSCFstart 0.001
end

*xyzfile 1 2 filename.xyz

%eprnmr
   nuclei = 10 { aiso, adip, aorb, fgrad }
   nuclei = 11 { aiso, adip, aorb, fgrad }
   nuclei = 12 { aiso, adip, aorb, fgrad }
   nuclei = 83 { aiso, adip, aorb, fgrad }
end
```

References

(1) Pantazis, D. A.; Orio, M.; Petrenko, T.; Zein, S.; Bill, E.; Lubitz, W.; Messinger, J.; Neese, F. A New Quantum Chemical Approach to the Magnetic Properties of Oligonuclear Transition-Metal Complexes: Application to a Model for the Tetranuclear Manganese Cluster of Photosystem II. *Chem. Eur. J.* **2009**, *15*, 5108-5123.

(2) Cox, N.; Ames, W.; Epel, B.; Kulik, L. V.; Rapatskiy, L.; Neese, F.; Messinger, J.; Wieghardt, K.; Lubitz, W. Electronic Structure of a Weakly Antiferromagnetically Coupled $Mn^{II}Mn^{III}$ Model Relevant to Manganese Proteins: A Combined EPR, ^{55}Mn-ENDOR, and DFT Study. *Inorg. Chem.* **2011**, *50*, 8238-8251.

(3) Rapatskiy, L.; Ames, W. M.; Pérez-Navarro, M.; Savitsky, A.; Griese, J. J.; Weyhermüller, T.; Shafaat, H. S.; Högbom, M.; Neese, F.; Pantazis, D. A.; Cox, N. Characterization of Oxygen Bridged Manganese Model Complexes Using Multifrequency ^{17}O-Hyperfine EPR Spectroscopies and Density Functional Theory. *J. Phys. Chem. B* **2015**, *119*, 13904-13921.

(4) Schraut, J.; Kaupp, M. On Ammonia Binding to the Oxygen-Evolving Complex of Photosystem II: A Quantum Chemical Study. *Chem. Eur. J.* **2014**, *20*, 7300-7308.

(5) Lohmiller, T.; Krewald, V.; Navarro, M. P.; Retegan, M.; Rapatskiy, L.; Nowaczyk, M. M.; Boussac, A.; Neese, F.; Lubitz, W.; Pantazis, D. A.; Cox, N. Structure, ligands and substrate coordination of the oxygen-evolving complex of photosystem II in the S_2 state: a combined EPR and DFT study. *Phys. Chem. Chem. Phys.* **2014**, *16*, 11877-11892.